DALTON
FULL PAPER

Solid state coordination chemistry of oxovanadates: hydrothermal syntheses and structures of two novel copper vanadate ribbons, β-[Cu(2,2′-bipyridine)V_2O_6] and β-[Cu(2,2′:6′,2″-terpyridine)V_2O_6]†

Robert C. Finn,[a] Jessica Sims,[b] Chares J. O'Connor *[b] and Jon Zubieta *[a]

[a] *Department of Chemistry, Syracuse University, Syracuse, NY 13244, USA*
[b] *Advanced Materials Research Institute, University of New Orleans, New Orleans, LA 70148, USA*

Received 9th April 2001, Accepted 22nd October 2001
First published as an Advance Article on the web 10th December 2001

The hydrothermal reaction of $CuSO_4 \cdot 5H_2O$, Na_3VO_4, methylphosphonic acid, 2,2′-bipyridine, and H_2O in the mole ratio 1.22 : 1.30 : 3.63 : 1.00 : 2250 at 150 °C for 43 h yielded β-[Cu(bpy)V_2O_6] (**1**). The structure of **1** is a one-dimensional ribbon constructed of $\{V_6O_{18}\}^{6-}$ clusters linked by a binuclear subunit of edge sharing {Cu(bpy)O_3} square pyramids. Similarly, the reaction of Cu_2O, Na_3VO_4, 2,2′:6′,2″-terpyridine, selenous acid, and water, in a mole ratio 1.52 : 1.00 : 2.02 : 9.31 : 2130 at 200 °C for 67.5 h yielded β-[Cu(tpy)V_2O_6] (**2**). The structure of **2** is comprised of an undulating chain of corner sharing vanadium oxide tetrahedra, with $\{Cu(tpy)\}^{2+}$ subunits spanning the adjacent crests and troughs.

Introduction

The significant contemporary interest in inorganic oxide materials reflects their diverse physical properties with applications to catalysis, sorption, magnetism and photochemistry.[1,2] One approach to the design of novel materials exploits the influence of organic molecules on inorganic microstructures.[3,4] Zeolites,[5,6] mesoporous oxides of the MCM-41 class,[7] and open framework metal phosphates[8,9] are examples of materials which incorporate organic cations as structure-directing agents. An alternative approach to this method employs the organic component as a ligand, linking metal sites into complex metal–organic scaffoldings. A variant of this latter strategy utilizes a secondary metal subunit as a charge compensating, space-filling component and, in some instances, as intimate structural components of bimetallic oxide composite materials, exemplified by copper–molybdenum oxides such as [Cu(4,4′-bipyridylamine)MoO_4], [Cu (*o*-phen)MoO_4] and [{Cu(tetraphenylporphyrin)}$Cu_2Mo_3O_4$].[10–12] Considerable structural flexibility may be achieved through variations in ligand geometry, spatial extension and the coordination preferences of the secondary metal atom. The success of this approach and the evolution of a wealth of new materials in the molybdenum oxide family encouraged us to explore the structure-directing role of copper–organonitrogen subunits in the industrially significant vanadium oxide family of materials.

Vanadium oxides exhibit in most cases two-dimensional network structures.[13,14] Such layered inorganic oxides constitute a diverse class of materials most of which share the common structural motif of cationic guests, which reside between the anionic metal oxide layers. However, as noted above, the introduction of a secondary metal–ligand complex cation may have considerable influence on the microstructure of the oxide component. In this paper, the effects of bulk, denticity and π–π interactions of the ligand, as well as coordination preferences of the copper are discussed for the novel copper–vanadate materials β-[Cu(2,2′-bipyridine)(V_2O_6)] (**1**) and β-[Cu(terpyridine)(V_2O_6)] (**2**).

Results and discussion

Preparation and infrared spectra

The reaction of $CuSO_4 \cdot 5H_2O$, Na_3VO_4, methylphosphonic acid, 2,2′-bipyridine and H_2O in the mole ratio 1.22 : 1.30 : 3.63 : 1.00 : 2250 was carried out at 150 °C for 43 hours. Green crystals of compound **1** were isolated in 60% yield. Similarly, Cu_2O, Na_3VO_4, terpyridine, selenous acid and H_2O, in the mole ratio 1.52 : 1.00 : 2.02 : 9.31 : 2130 were reacted at 200 °C for 67.5 hours, yielding green crystals of compound **2** in 20% yield. Methylphosphonic acid in **1** as well as selenous acid in **2** are used to lower the pH in each reaction to *ca.* 3–4. Although these species do not appear in the final products, omission of the acid leads to an amorphous powder in each case. Different copper(II) and copper(I) sources were introduced in the synthesis of compound **2** and were found to form amorphous powders. In the preparation of **2**, copper(I) was oxidized to copper(II) with concomitant reduction of excess vanadium(V) to the +4 oxidation state which results in an overall lower yield of **2**. The infrared spectra of **1** and **2** exhibit strong bands in the 950–1000 cm^{-1} region characteristic of ν(V=O), as well as broad peaks above 3000 cm^{-1} and medium peaks at *ca.* 1600 cm^{-1} characteristic of aromatic ν(C–H, C–C) stretching. Bands at 784 cm^{-1} in **1** and 826 cm^{-1} in **2** are assigned to ν(V–O) for the bridging oxo-groups.

Structures

As shown in Fig. 1, the structure of **1** consists of copper–vanadium oxide ribbons, decorated with 2,2′-bipyridine groups projecting above and below the chain. The ribbon is constructed from rings of corner-sharing vanadium(V) tetrahedra linked through square pyramidal edge-sharing copper(II) dimers. The ribbon is further decorated with distorted square planar $\{Cu(bpy)\}^{2+}$ subunits bound to the vanadium rings. The

† Electronic supplementary information (ESI) available: polyhedral representation of the $\{V_6O_{18}\}^{6-}$ unit in [(H_2en)(MnF)(VO_3)$_3$]; structure of [(H_2dn)(MnF)(VO_3)$_3$]; polyhedral representation of [Zn(tpy)$_2V_6O_{17}$]; polyhedral representations of α-[Cu(bpy)V_2O_6], [Cu(bpy)$_2V_2O_6$], {Cu(H_2en)V_2O_6] and α-[Cu(tpy)V_2O_6]. See http://www.rsc.org/suppdata/dt/b1/b103165c/

DOI: 10.1039/b103165c

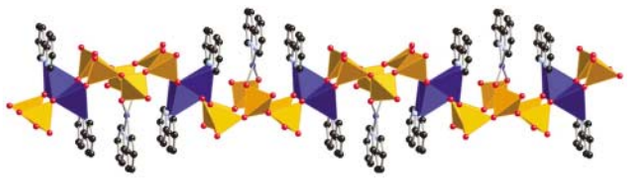

Fig. 1 A polyhedral representation of the structure of β-[Cu(bpy)-V_2O_6] (**1**), normal to the ribbon. Red spheres, oxygen; dark blue sites, copper; orange sites, vanadium; light blue spheres, nitrogen; black spheres, carbon. Hydrogen atoms have been omitted for clarity.

Cu(II) square pyramidal coordination geometry is defined by the nitrogen donors of the bpy ligand, one triply bridging oxo-groups, and one doubly bridging oxo-groups defining the basal plane, as well as one triply bridging oxo-groups in the apical position. The square planar copper subunit bridges to the two central vanadium tetrahedra of the ring. The vanadium tetrahedra form a cyclic, corner-sharing hexanuclear subunit. The two central vanadium tetrahedra are defined by two V–O–V bridging oxo-groupss, one V–O–$Cu_{sq.\ pl.}$ bridging oxo-groups and one terminal oxo-groups (see Table 1). The four peripheral

Table 1 Bond lengths (Å) and angles (°) for β-[Cu(bpy)V_2O_6] (**1**)

Cu(1)–O(2)	1.943(5)	V(3)–O(3)	1.787(5)
Cu(1)–O(1)	1.971(5)	V(3)–O(5)	1.796(5)
Cu(1)–N(2)	1.980(7)	V(4)–O(9)	1.622(6)
Cu(1)–N(1)	1.995(6)	V(4)–O(8)	1.694(5)
Cu(1)–O(1)#1	2.368(5)	V(4)–O(7)	1.777(5)
Cu(2)–O(8)	1.911(5)	V(4)–O(3)#2	1.788(6)
Cu(2)–O(8)#2	1.911(5)	V(5)–O(6)	1.608(5)
Cu(2)–N(3)	1.965(6)	V(5)–O(2)	1.681(5)
Cu(2)–N(3)#2	1.965(6)	V(5)–O(5)	1.819(5)
V(3)–O(4)	1.620(5)	V(5)–O(7)	1.819(5)
V(3)–O(1)	1.703(5)		
O(2)–Cu(1)–O(1)	93.0(2)	O(3)–V(3)–O(5)	109.3(3)
O(2)–Cu(1)–N(2)	92.2(2)	O(9)–V(4)–O(8)	108.5(3)
O(1)–Cu(1)–N(2)	174.6(2)	O(9)–V(4)–O(7)	108.3(3)
O(2)–Cu(1)–N(1)	172.5(2)	O(8)–V(4)–O(7)	110.7(3)
O(1)–Cu(1)–N(1)	92.8(2)	O(9)–V(4)–O(3)#2	109.5(3)
N(2)–Cu(1)–N(1)	82.0(3)	O(8)–V(4)–O(3)#2	111.8(3)
O(8)–Cu(2)–N(3)	97.0(2)	O(7)–V(4)–O(3)#2	108.0(2)
O(8)#2–Cu(2)–N(3)	159.6(2)	O(6)–V(5)–O(2)	110.1(3)
O(4)–V(3)–O(1)	108.8(3)	O(6)–V(5)–O(5)	111.0(3)
O(4)–V(3)–O(3)	111.0(3)	O(2)–V(5)–O(5)	107.4(2)
O(1)–V(3)–O(3)	110.2(2)	O(6)–V(5)–O(7)	109.6(3)
O(4)–V(3)–O(5)	109.4(3)	O(2)–V(5)–O(7)	109.9(2)
O(1)–V(3)–O(5)	108.1(2)	O(5)–V(5)–O(7)	108.8(2)

Symmetry transformations used to generate equivalent atoms: #1 $-x$, $-y$, $-z$. #2 $-x$, y, $-z + 1/2$.

vanadium tetrahedra have two distinct environments; two vanadiums have two V–O–V bridging oxo-groupss, one doubly bridging V–O–Cu oxo-groups and one terminal oxo-groups; the remaining environment differs in its coordination to the copper square pyramids, in that one oxo-groups is triply bridging to both coppers of the binuclear unit.

The structure of **1** may be described as $\{V_6O_{18}\}^{6-}$ corner-sharing hexanuclear rings linked through $\{Cu(bpy)\}_2^{4+}$ dimers to form a one-dimensional ribbon of two polyhedra thickness. The presence of the additional, square planar $\{Cu(bpy)\}^{2+}$ subunit is required as a charge compensating cation. The location of this Cu(II) site on the chain may reflect aromatic π-stacking effects, such that the crowning of the $\{V_6O_{18}\}^{6-}$ ring accommodates the interdigitation of ligands across ribbons. It is noteworthy that the $\{V_6O_{18}\}^{6-}$ hexanuclear ring has been observed previously in hydrothermally prepared vanadates,[15,16] of which $[(H_2en)(MnF)(VO_3)_3]$ is characteristic. The structure of $[(H_2en)(MnF)(VO_3)_3]$ is more closely packed than that of **1** due to the relative size of ethylenediamine, and the absence of a copper site spanning the central tetrahedra of the vanadium ring. A somewhat different manifestation of the hexavanadate ring is observed in $[\{Zn(terpy)\}_2V_6O_{17}]$. In this structure the vanadium rings fuse to form isolated one-dimensional ribbons, which are linked through $\{Zn(terpy)\}^{2+}$ secondary metal cations to form a two-dimensional sheet. The presence of a common structural motif in much different overall architectures reflects the structural versatility inherent in such hydrothermally prepared metastable phases.

As shown in Fig. 2a, compound **2** can be described as copper–

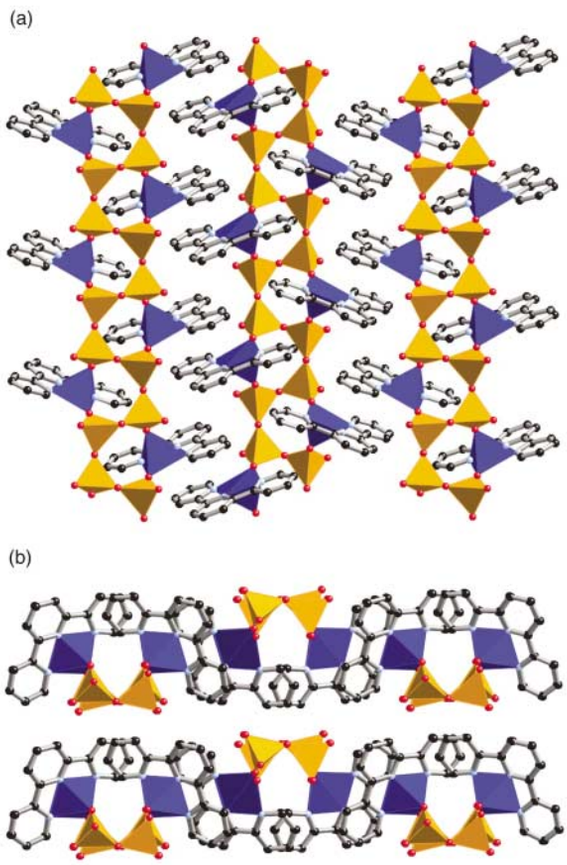

Fig. 2 (a) A polyhedral view of three ribbons, normal to the direction of propagation, showing the "herringbone" pattern for β-[Cu(tpy)-V_2O_6] (**2**). (b) A view parallel to the direction of the ribbons showing the "encapsulation" of the oxide chain.

vanadium oxide ribbons decorated with terpyridine ligands projecting into the region between the chains. Closer inspection of the structure reveals the undulating vanadium oxide chain, with amplitude of one tetrahedron and a periodicity of four tetrahedra. The vanadate tetrahedra of the chains are also bridged at the trough and the crest of the wave by the $\{Cu(terpy)\}^{2+}$ subunits, which fill the gaps in the two polyhedra thick ribbon. The presence of the $\{Cu(terpy)\}^{2+}$ subunit also generates a unique, ten membered ring, $\{CuV_4O_5\}$. The nitrogen donors of the terpy ligand and one bridging oxo-group define the basal plane for the copper site; a second bridging oxo-group defines the apical position and completes the square pyramidal coordination geometry. The tetrahedral vanadium sites exhibit identical coordination geometries: two V–O–V bridging oxo-groups, one V–O–Cu bridging oxo-group, and one terminal oxo-group (see Table 2).

One consequence of the square pyramidal coordination about the copper is an angular canting of terpyridine toward the ribbon edge. This canting results in a distance between parallel aromatic rings of adjacent chains of 3.4 Å, indicating the presence of significant face to face π–π stacking.[17] This strong interaction may be a driving force for adopting the canted chain structure. In Fig. 2a, the aromatic ligands stack in a "herringbone" pattern. If the structure is viewed down the

Table 2 Bond lengths (Å) and angles (°) for β-[Cu(tpy)V_2O_6] (**2**)

Cu(1)–O(2)	1.889(3)	V(2)–O(3)	1.783(3)
Cu(1)–N(2)	1.937(3)	V(2)–O(5)	1.787(3)
Cu(1)–N(3)	2.038(3)	V(3)–O(6)	1.628(3)
Cu(1)–N(1)	2.039(3)	V(3)–O(1)#1	1.654(3)
Cu(1)–O(1)	2.140(3)	V(3)–O(3)#2	1.800(3)
V(2)–O(4)	1.619(3)	V(3)–O(5)	1.807(3)
V(2)–O(2)	1.680(3)		
O(2)–Cu(1)–N(2)	163.43(14)	O(4)–V(2)–O(5)	107.95(15)
O(2)–Cu(1)–N(3)	97.73(13)	O(2)–V(2)–O(5)	111.60(14)
N(2)–Cu(1)–N(3)	79.71(14)	O(3)–V(2)–O(5)	109.38(14)
O(2)–Cu(1)–N(1)	99.85(13)	O(6)–V(3)–O(1)#1	109.63(15)
N(2)–Cu(1)–N(1)	80.25(14)	O(6)–V(3)–O(3)#2	110.45(15)
N(3)–Cu(1)–N(1)	159.16(14)	O(1)#1–V(3)–O(3)#2	106.75(15)
O(2)–Cu(1)–O(1)	100.71(12)	O(6)–V(3)–O(5)	108.17(14)
N(2)–Cu(1)–O(1)	95.62(13)	O(1)#1–V(3)–O(5)	111.65(14)
N(3)–Cu(1)–O(1)	88.98(12)	O(3)#2–V(3)–O(5)	110.21(14)
N(1)–Cu(1)–O(1)	98.62(12)	V(3)#2–O(1)–Cu(1)	134.17(17)
O(4)–V(2)–O(2)	110.26(15)	V(2)–O(2)–Cu(1)	165.87(18)
O(4)–V(2)–O(3)	110.11(16)	V(2)–O(3)–V(3)#1	144.4(2)
O(2)–V(2)–O(3)	107.55(15)	V(2)–O(5)–V(3)	128.99(17)

Symmetry transformations used to generate equivalent atoms: #1 $x, -y + 1/2, z - 1/2$. #2 $x, -y + 1/2, z + 1/2$.

metal oxide chain, as in Fig. 2b, the bimetallic oxide chains are encapsulated by an undulating ligand pattern. It becomes apparent that the hydrophobicity, as well as the bite angle of terpyridine, are controlling factors in hindering the propagation of the metal oxide in more than one-dimension.

Although structures **1** and **2** are both one-dimensional chains, it is noteworthy that terpyridine, the ligand of increased bulk and denticity, is associated with the structure of higher vanadate dimensionality, that is, the one-dimensional chain of **2**, while the bipyridine ligand is associated with the hexanuclear rings or zero-dimensionality vanadate substructure of **1**. It is noteworthy that in previously reported materials, changing ligand denticity and steric bulk, such as with bpy and terpy has, not unexpectedly, led to different dimensionalities for overall structures: for example, the two-dimensional [{Cu(bpy)}$_2$-$(VO)_3(PO_4)_2(HPO_4)_2$]·$2H_2O$ and the one-dimensional [{Cu-(terpy)}$_2$$(VO_2)_3(PO_4(HPO_4)_2]$.[18]

The structures of this study represent two additional compounds in a growing list of one- and two-dimensional copper polyimine vanadates.[19,20] For the previously reported bipyridine compounds α-[Cu(bpy)V_2O_6] and [Cu(bpy)$_2V_2O_6$], the structures vary considerably, although both propagate as one-dimensional vanadate chains. However, due to multiple ligands bonding to each copper in [Cu(bpy)$_2V_2O_6$], the {Cu(bpy)$_2$}$^{2+}$ square pyramids only exhibit limited accessibility to the coordination sphere for additional ligands, allowing for a more open, undulating vanadium chain. In contrast in α-[Cu(bpy)-V_2O_6], the facile accessibility of coordination sites at the {Cu(bpy)}$^{2+}$ site allows two vanadate chains to link together through the square pyramidal copper centers to form the one-dimensional ribbon.

Exploiting a smaller ligand, like ethylenediamine, provides additional space around the copper for further, albeit rather long-range interactions, which reflect the "4 + 1" and "4 + 2" geometries associated with Jahn–Teller distortions at the d^9 metal center. This is evident in [Cu(H_2en)V_2O_6] where double chains of corner sharing vanadium oxide tetrahedra are linked through {Cu(en)}$^{2+}$ sites into a two-dimensional network. This bonding motif most resembles α-[Cu(bpy)V_2O_6]; however, without the spatial restrictions of the bipyridine ligands, [Cu-(H_2en)V_2O_6] is able to extend into two-dimensions. Finally, α-[Cu(terpy)V_2O_6] is composed of one-dimensional undulating vanadate chains linked through {Cu(terpy)}$^{2+}$ binuclear units to form a two-dimensional network. The network structure was unanticipated, since the tridentate and sterically demanding terpyridine ligand was expected to passivate the secondary metal with respect to bridging in two-dimensions as observed for the β-[Cu(terpy)V_2O_6] isomer **2**. However, the formation of the binuclear {Cu_2(terpy)$_2O_4$} subunit allows bridging between the vanadate chains.

Magnetic studies

Since both **1** and **2** contain Cu(II), with a d^9 electronic configuration, and V(V), a d^0 species, one unpaired electron (S = 1/2) at each copper site contributes to the magnetic behavior in each case. The value of χ for β-[Cu(bpy)V_2O_6] (**1**) was small and positive ranging from $\chi = 10^{-4}$ to 10^{-6}. In this case, the zero field cooled (zfc) and field cooled (fc) DC susceptibility curves were identical and paramagnetic (Fig. 3). The paramagnetic behavior

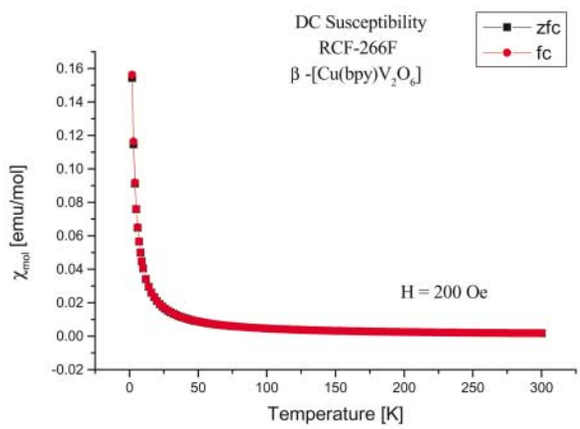

Fig. 3 Temperature dependence of χ_m for **1** between 2 and 300 K. The squares and circles represent zero-field-cooled (zfc) and field-cooled (fc) data, respectively.

was inversely proportional to temperature as predicted by the Curie–Weiss law and plotted in Fig. 4:

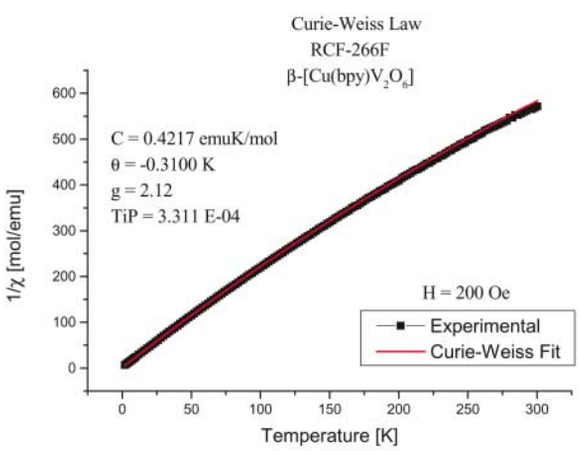

Fig. 4 Curie–Weiss law fit for the susceptibility of **1**.

$$\chi = \frac{C}{T-\theta} = \frac{Ng^2\mu_B{}^2 S(S+1)}{3k_B(T-\theta)} + \mathrm{TiP}$$

where C = the Curie constant, T = temperature and θ = the Weiss constant, N = Avogadro's number, g = Lande splitting, μ_B = Bohr magneton, S = electron spin, k_B = Boltzmann's constant, and TiP = temperature independent paramagnetism.[21–23] The best-fit nonlinear regression values were obtained by the Levenberg–Marquardt method. The best fitted values were C = 0.4217 emu K mol^{-1}, $\theta = -0.3100$ K, g = 2.12 and TiP = 3.31 × 10^{-4} emu mol^{-1} (R^2 = 1). The effective magnetic moment (μ_{eff}) was plotted as a function of temperature to further determine the existence of coupling interactions between paramagnetic spins. Here, μ_{eff} was defined by the following equation:

$$\mu_{eff} = (8\chi T)^{1/2}$$

The plot, shown in Fig. 5, demonstrated antiferromagnetic

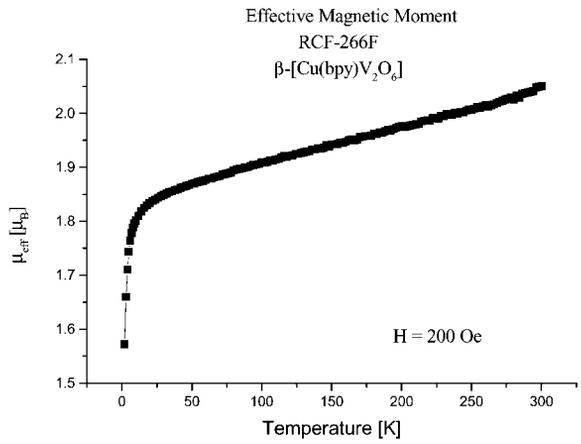

Fig. 5 A plot of the effective moment of **1** as a function of temperature.

coupling of paramagnetic spins as seen by the descent of μ_{eff} at low temperatures. The effective magnetic moment varies from 1.85 to 2.05 μ_B.

For β-[Cu(terpy)V_2O_6] (**2**), the zfc and fc DC susceptibility curves were also identical and paramagnetic at high temperatures, with χ ranging from 10^{-3} to 10^{-6} (Fig. 6). A Curie–Weiss

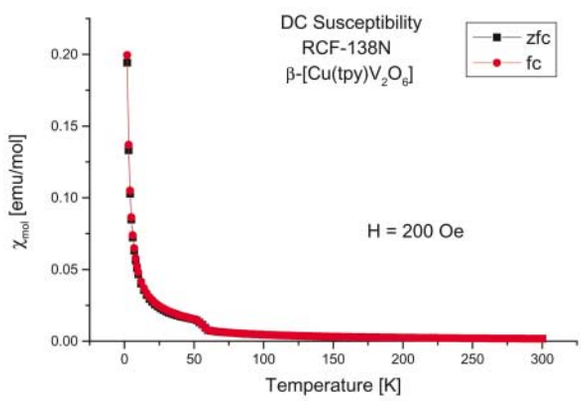

Fig. 6 Temperature dependence of χ_m for **2** between 2 and 300 K. The squares and circles represent zero-field-cooled (zfc) and field-cooled (fc) data, respectively.

fit in the range 100 to 300 K gave $C = 0.4468$ emu K mol^{-1}, $\theta = -5.719$ K, $g = 2.18$ and TiP = 2.32×10^{-4} emu mol^{-1} (Fig. 7).

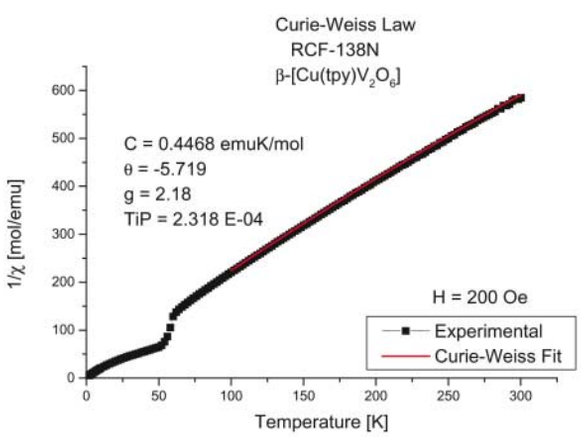

Fig. 7 Curie–Weiss law fit in the range 100 to 300 K for **2**.

The anomaly observed at *ca.* 60 K exhibits only minor changes upon increasing the field strength from 20 to 200 to 2000 Oe, suggesting a possible non-magnetic origin such as a phase change (Fig. 8).

Thermal analysis

The TGA of **1** showed no weight change below 310 °C. Between 310 and 425 °C, a weight loss of 36.8% corresponding to the loss of ligand (37.4% calculated) is observed. The blue-gray residue is a mixture of β-$Cu_2V_2O_7$ and V_2O_5. The TGA of **2** indicated that the terpy ligand is lost in two stages with weight loses of 15% at 270–340 °C and 30% at 340–420 °C (47.1%, calculated for the loss of terpyridine).

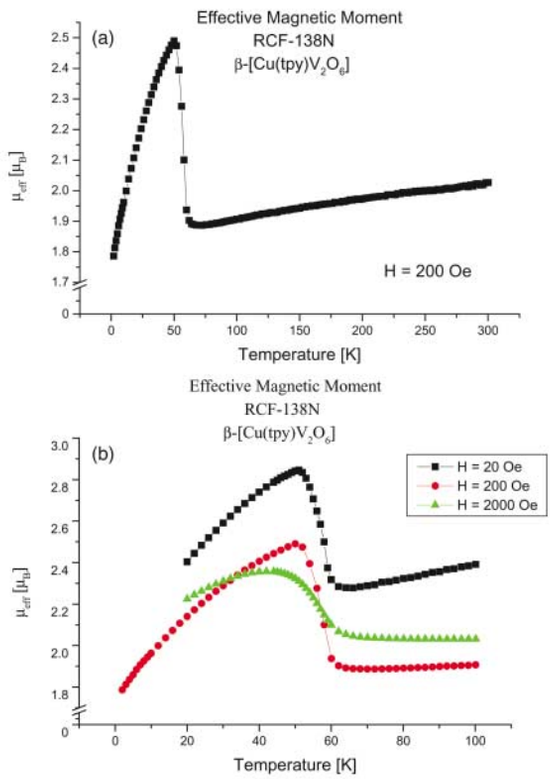

Fig. 8 (a) A plot of the effective magnetic moment of **2** as a function of temperature. (b) The effective magnetic moment of **2** at 20, 200, and 2000 Oe between 2 and 100 K.

Conclusions

The title compounds as well as the four previously reported materials, are representative of the growing number of vanadium oxide structures incorporating secondary metal complex cations. The structural diversity of vanadium oxides in the hydrothermal regime is apparent. The ease of substituting ligands as well as secondary metals is evident in the network structures of the previously reported materials, [{M(bpy)}$_2$-$V_{12}O_{32}$] (M = Ni, Co, Cu) and [Ni(dien)(V_2O_6)].[20,24]

Vanadium oxides have received considerable attention due to their diverse physical properties.[25] Significant activity has focused on structural modification and design of vanadium oxides through the introduction of organic substructures as templates and charge compensating cations.[26] The approach to hybrid bimetallic oxide/organic solids, illustrated by the isolation of **1** and **2**, utilizes secondary metal–ligand subunits as covalent linkers to the vanadium oxide substructure. The evolution of synthetic design in such solids exploits the systematic variation of the secondary metal, its coordination preferences, the organic ligand, and the hydrothermal reaction conditions. However, continued development in an empirical fashion is required to provide a data base for rationalizing structure–property relationships of these materials.

Table 3 Summary of crystal data and structure refinement for β-[Cu(bpy)V_2O_6] (**1**) and β-[Cu(tpy)V_2O_6] (**2**)

Compound	β-[Cu(bpy)V_2O_6]	β-[Cu(tpy)V_2O_6]
Empirical formula	$C_{30}H_{24}Cu_3N_6O_{18}V_6$	$C_{15}H_{11}CuN_3O_6V_2$
Formula weight	1251.81	494.69
Crystal size/mm	0.34 × 0.16 × 0.14	0.28 × 0.09 × 0.07
Crystal system	Monoclinic	Monoclinic
Space group	*C*2/*c*	$P2_1/c$
a/Å	18.973(2)	9.3222(7)
b/Å	10.568(1)	21.299(6)
c/Å	19.633(2)	8.3524(6)
β/°	94.565(2)	92.787(2)
Volume/Å^3	39.24.0(8)	1656.5(2)
Z	4	4
D_{calc}/g cm^{-3}	2.121	1.984
F(000)	2460	980
λ/Å	0.71073	0.71073
μ/mm^{-1}	3.038	2.418
Unique data	4704	4001
Final *R* indices		
*R*1 (*wR*2)	0.0689 (0.1600)	0.0450 (0.0958)

Experimental

Reactions were carried out in 23 ml polytetrafluoroethylene-lined stainless steel containers under autogenous pressure. Reagents were purchased from Aldrich Chemicals and used without further purification. Distilled water was purified to below 3.0 Ω in-house with a Barnstead Model 525 Biopure system.

Synthesis

β-[Cu(bpy)V_2O_6] (1). A solution of $CuSO_4 \cdot 5H_2O$ (0.076 g, 0.304 mmol), Na_3VO_4 (0.060 g, 0.326 mmol), methylphosphonic acid (0.087 g, 0.906 mmol), 2,2′-dipyridyl (0.039 g, 0.250 mmol) and H_2O (10.16 g, 564 mmol) in the mole ratio of 1.22 : 1.30 : 3.63 : 1.00 : 2250 was carried out at 150 °C for 43 hours. After cooling to room temperature green crystals of β-[Cu(bpy)V_2O_6] were isolated in 60% yield. IR (KBr pellet, cm^{-1}) 2346 (s), 1686 (m), 1654 (m), 1601 (m), 1560 (w), 1508 (m), 1498 (m), 1447 (s), 986 (br), 950 (br), 784 (m).

β-[Cu(terpy)V_2O_6] (2). A solution of Cu_2O (0.057 g, 0.398 mmol), Na_3VO_4 (0.048 g, 0.261 mmol), terpyridine (0.123 g, 0.527 mmol), selenous acid (0.313 g, 2.43 mmol) and H_2O (10.02 g, 556 mmol), in the mole ratio 1.52 : 1.00 : 2.02 : 9.31 : 2130 was heated at 200 °C for 67.5 hours. After cooling to room temperature green crystals of β-[Cu(terpy)V_2O_6] were isolated in 20% yield. IR (KBr pellet, cm^{-1}) 2345 (m), 1600 (m), 1449 (s), 1022 (m), 942 (br), 826 (br), 638 (m).

X-Ray crystallography

Crystallographic data (Table 3) were collected with a Siemens P4 diffractometer equipped with a SMART CCD 1K system[27] and using Mo-Kα radiation (*λ* = 0.71073 Å). The data were collected at 90(3) K and corrected for Lorentz and polarization effects. Absorption corrections were made using SADABS.[28] The structure solution and refinement were carried out using the SHELXL97[29] software package. The structures were solved using direct methods and all of the non-hydrogen atoms were located from the initial solution. After locating all of the non-hydrogen atoms in each structure, the model was refined against F^2, initially using isotropic, and later anisotropic, thermal displacement parameters until the final value of Δ/σ_{max} was less than 0.001.

CCDC reference numbers 171061 and 171062.

See http://www.rsc.org/suppdata/dt/b1/b103165c/ for crystallographic data in CIF or other electronic format.

Magnetic susceptibility studies

Magnetic susceptibility measurements were performed on a Quantum Design MPMS-5 system with a Superconducting Quantum Interference Device (SQUID) detector. Detailed magnetic susceptibility measurement theory and instrumental calibration techniques are discussed elsewhere.[21] GraphPad Prism Version 3.02 by GraphPad Software Inc. was used to compute all nonlinear regression fits.

DC susceptibility measurements were obtained in zero-field cooled (zfc) and field cooled (fc) experiments at an applied field (*H*) of 200 Oe for both samples. Additional field cooled experiments were executed for β-[Cu(tpy)V_2O_6] at H = 20 Oe and H = 2000 Oe. For each case, a magnetic moment was obtained and converted into susceptibility (χ) in cgs units.

Acknowledgements

This work was supported by NSF grant CHE9987471.

References

1 D. W. Bruce and D. O'Hare (Editors), *Inorganic Materials*, Wiley, Chichester, 1992.
2 A. J. Cheetham, *Science*, 1994, **264**, 794 and references therein.
3 S. I. Stupp and P. V. Braun, *Science*, 1997, **277**, 1242.
4 P. V. Braun, P. Osemar, V. Tohver, S. B. Kennedy and S. I. Stupp, *J. Am. Chem. Soc.*, 1999, **121**, 7302.
5 D. E. W. Vaughn, *Properties and Applications of Zeolites, Chemical Society Special Publication, No. 33*, ed. R. P. Townsend, The Chemical Society, London, 1979, p. 294.
6 M. E. Davis and R. F. Lobo, *Chem. Mater.*, 1992, **4**, 756.
7 C. T. Kresge, M. E. Leonowicz, W. J. Roth, J. C. Vartuli and J. S. Beck, *Nature (London)*, 1992, **359**, 710.
8 M. I. Khan, L. M. Meyer, R. C. Haushalter, C. L. Sweitzer, J. Zubieta and J. L. Dye, *Chem. Mater.*, 1996, **8**, 43.
9 P. Feng, X. Bu and G. D. Stucky, *Nature (London)*, 1997, **388**, 735.
10 P. J. Hagrman, D. Hagrman and J. Zubieta, *Angew. Chem., Int. Ed.*, 1999, **38**, 2638.
11 D. J. Chesnut, D. Hagrman, P. J. Zapf, R. P. Hammond, R. La Duca, Jr., R. C. Haushalter and J. Zubieta, *Coord. Chem. Rev.*, 1999, **190–192**, 737.
12 D. Hagrman, P. J. Hagrman and J. Zubieta, *Angew. Chem., Int. Ed.*, 1999, **38**, 3615.
13 P. J. Hagrman, R. C. Finn and J. Zubieta, *Solid State Sci.*, 2001, **3**, 745.
14 P. Y. Zavalij and M. S. Whittingham, *Acta Crystallogr., Sect. B*, 1999, **55**, 627 and references therein.
15 T. S.-C. Law and I. D. Williams, *Chem. Mater.*, 2000, **12**, 2070.
16 P. J. Hagrman and J. Zubieta, *Inorg. Chem.*, 2000, **39**, 3252.
17 M. Munakata, L. P. Wu, M. Yamamoto, T. Kuroda-Sowa and M. Maekawa, *J. Am. Chem. Soc.*, 1996, **118**, 3117 and references therein.
18 R. Finn and J. Zubieta, *Chem. Commun.*, 2000, **14**, 1321.
19 J. R. D. DeBord, Y. Zhang, R. C. Haushalter, J. Zubieta and C. J. O'Connor, *J. Solid State Chem.*, 1996, **122**, 251.
20 L.-M. Zheng, J.-S. Zhao, K.-H. Lii, L.-Y. Zhang, Y. Liu and X.-Q. Xin, *J. Chem. Soc., Dalton Trans.*, 1999, 939.
21 C. J. O'Connor, *Prog. Inorg. Chem.*, 1982, **29**, 202.
22 C. J. O'Connor (Editor), *Research Frontiers in Magnetochemistry*, World Scientific, New Jersey, 1993.
23 D. Jiles, *Introduction to Magnetism and Magnetic Materials*, Chapman and Hall, New York, 1991.
24 P. J. Ollivier, J. R. D. DeBord, P. J. Zapf, J. Zubieta, L. M. Meyer, C.-C. Wang, T. E. Mallouk and R. C. Haushalter, *J. Mol. Struct.*, 1998, **470**, 49.
25 Y. Zhang, J. R. D. DeBord, C. J. O'Connor, R. C. Haushalter, A. Clearfield and J. Zubieta, *Angew. Chem., Int. Ed. Engl.*, 1996, **35**, 989.
26 P. J. Hagrman, C. Bridges, J. E. Greedan and J. Zubieta, *J. Chem. Soc., Dalton Trans.*, 1999, 2901.
27 Siemens "Smart" Software Reference Manual, Siemens Analytical X-Ray Instruments, Inc., Madison, Wisconsin, 1994.
28 G. M. Sheldrick, SADABS, Program for Empirical Absorption Corrections, University of Gottingen, Germany, 1996.
29 G. M. Sheldrick, SHELXL97, Program for the Refinement of Crystal Structures, University of Gottingen, Germany, 1997.